NUCLEAR SCIENCE AND ENGINEERING: **179**, 1–10 (2015)

Lead Slowing-Down Spectrometry Analysis of Data from Measurements on Nuclear Fuel

Glen A. Warren,* Kevin K. Anderson, and Jonathan Kulisek

Pacific Northwest National Laboratory
Richland, Washington 99352

Yaron Danon and Adam Weltz

Rensselaer Polytechnic Institute
Troy, New York 12180

A. Gavron

Los Alamos National Laboratory
Los Alamos, New Mexico 87545

and

Jason Harris and Trevor N. Stewart

Idaho State University
Pocatello, Idaho 83204

Received September 11, 2013
Accepted June 17, 2014
http://dx.doi.org/10.13182/NSE13-71

Abstract—*Improved nondestructive assay of isotopic masses in used nuclear fuel would be valuable for nuclear safeguards operations associated with the transport, storage, and reprocessing of used nuclear fuel. Our collaboration is examining the feasibility of using lead slowing-down spectrometry techniques to assay the isotopic fissile masses in used nuclear fuel assemblies. We present the application of our analysis algorithms to measurements conducted with a lead spectrometer. The measurements involved a single fresh fuel pin and discrete ^{239}Pu and ^{235}U samples. We are able to describe the isotopic fissile masses with root-mean-square errors over seven different configurations to 6.3% for ^{239}Pu and 2.7% for ^{235}U. Significant effort is yet needed to demonstrate the applicability of these algorithms for used-fuel assemblies, but the results reported here are encouraging in demonstrating that we are making progress toward that goal.*

I. INTRODUCTION

An understanding of the isotopic fissile masses in used-fuel assemblies is important for a variety of nuclear safeguards operations. Fissile content in *used fuel* impacts how it is transported, stored, and reprocessed. Nondestructive assay (NDA) techniques can be used to measure the fissile content for determining shipper-receiver differences and to retain or recover continuity of knowledge. Current NDA techniques infer total plutonium mass using a combination

*E-mail: glen.warren@pnnl.gov

of burnup codes for calculating isotopic inventories and passive measurements of easily measured isotopes in used fuel (e.g., ^{137}Cs and ^{244}Cm) to confirm the burnup calculations. The International Atomic Energy Agency (IAEA) has determined that these methods are capable of estimating the plutonium mass to within $\sim$10% (Ref. 1). The ability to directly measure plutonium in used fuel with greater certainty than current methods has been identified as a need for nuclear safeguards.[2] Furthermore, a more accurate technique that directly measures the individual fissile material masses in used-fuel assemblies without operator-provided information could be of great benefit in rectifying accounting errors in the fissile material mass as well as in improving our ability to detect diversion.

The MPACT (Material Protection, Accounting, and Control Technology) Campaign within the U.S. Department of Energy is funding research to develop methods for the accurate, direct, and independent assay of fissile isotopes in bulk materials such as used-fuel assemblies for the next-generation domestic nuclear fuel cycle. As part of this campaign, our collaboration will investigate the application of lead slowing-down spectrometry (LSDS) for the direct measurement of plutonium in used-nuclear-fuel assemblies. LSDS is a mature, active interrogation technique having a long and extensive history for use in nuclear cross-section measurements.[3–4] The goal of this effort is to use LSDS to directly measure fissile isotopes (e.g., ^{235}U, ^{239}Pu, and ^{241}Pu) in used-fuel assemblies with $<3\%$ uncertainty per isotope with minimal externally provided (operator-declared) information and in a time-efficient manner (i.e., within tens of minutes). If successful, we will improve on existing techniques by providing mass information per isotope without operator-provided information. Direct measurement of fissile isotopes using a technique such as LSDS would be particularly useful at the input of a reprocessing facility or to conduct final assay before fuel enters long-term storage.

In earlier work, the potential of LSDS techniques was demonstrated by applying an algorithm to extract fissile isotopic masses from simulated measurements on used-fuel assemblies.[5] The algorithm, based on singular value decomposition (SVD), was labeled as "semiempirical" because of its reliance on a combination of a basic physics description of the measurement process and a set of calibration measurements. The simulations of the measurements were calculated using MCNPX (Ref. 6) to model the LSDS process. To ensure that a wide variety of different fuel characteristics was studied, as well as to understand systematic uncertainties, simulations were calculated for LSDS assays of the Next Generation Safeguards Initiative (NGSI) 64 and NGSI 27 diversion used-fuel-assembly models.[7] The SVD semiempirical method requires the use of isotopic fission chambers lined with fissile isotopes assumed to be present in the used fuel (e.g., ^{235}U, ^{239}Pu, and ^{241}Pu). These isotopic fission chambers measure the energy and time-broadened fission cross sections to deconvolve the assay signal from the threshold fission chambers. The combined ^{239}Pu and ^{241}Pu mass estimates from these simulated LSDS assays were within a relative mean absolute deviation of 1.4% on the NGSI 64 fuel assemblies and 1.2% for the NGSI 27 diversion assemblies.[5] Note that these deviations do not reflect all of the uncertainties of an actual measurement, e.g., uncertainties in calibration masses and in normalization.

In 2012, Pacific Northwest National Laboratory (PNNL) developed both linear and quadratic purely empirical models that require only a threshold fission chamber signal to estimate the isotopic masses.[8] A threshold fission chamber is predominantly sensitive to fast neutrons, such as those emitted from fission reactions. Like the SVD semiempirical model, these models also involve a calibration procedure using a set of used-fuel assemblies with well-known masses.

Most of the LSDS algorithm development effort reported to date has involved the use of radiation transport modeling simulations of data. The focus of this paper is the application of those algorithms to measurement data collected in 2012 by Rensselaer Polytechnic Institute (RPI) using its lead spectrometer facility. Various measurements were conducted on a fresh special power excursion reactor test (SPERT) pin and a set of ^{239}Pu and ^{235}U samples. These experiments provided a limited set of real LSDS data to benchmark the analysis algorithms for determining the ^{239}Pu and ^{235}U in the samples.

This paper is presented in the following order. The next section introduces the concepts of LSDS. Then, a description of the RPI measurements is provided, followed by a description of the analysis algorithms. We then present our results and conclusions from the application of the LSDS analysis algorithms to the RPI data.

II. PRINCIPLES OF LSDS

The operation of a lead spectrometer relies primarily on two aspects. First, the unique and strong neutron energy-dependent resonance structure of the fission cross sections of isotopes within the assay sample provides a signature for assay. Second, the relationship between time and neutron energy that develops after a pulse of neutrons is injected into the lead provides a means to measure that isotopic-specific signature through measuring the timing of the fission neutrons. A lead spectrometer consists of a large stack of high-purity lead, a neutron source, and various sensors to detect the neutrons of interest. A simplified cross-section schematic of the RPI lead spectrometer is shown in Fig. 1 as an example. This spectrometer uses a linear electron accelerator (LINAC) to generate an electron beam. This beam impinges on a

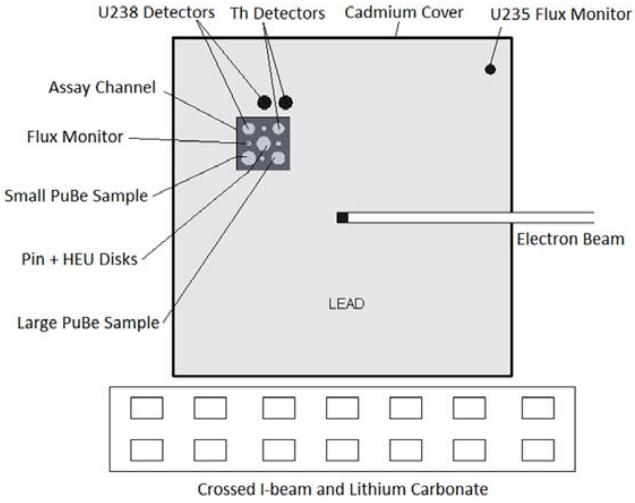

Fig. 1. Diagram of the RPI LSDS. Diagram from Ref. 9.

tantalum target to generate a neutron pulse in the center of the lead spectrometer. The sample is placed in the LSDS channel. A more detailed description of the experimental setup will be provided in Sec. III.

To start the process, a pulse of interrogation neutrons with initial energies of at least several hundred kilo-electron-volts is injected into the lead spectrometer. These interrogating neutrons lose energy quickly through inelastic scattering with the lead nuclei. At 1 μs after the pulse, the neutron energy decreases to <100 keV, and the scattering interaction becomes predominantly elastic in nature. Since the lead elastic scattering cross section is fairly constant below several tens of kilo-electron-volts and the interaction rate is proportional to the neutron velocity, the neutron energy distribution becomes focused at these energies. The energy distribution can be approximated by a Gaussian distribution with a full-width at half-maximum of approximately one-third the mean neutron energy.[7] Because of the large relative mass of the lead nuclei compared with that of a neutron, the neutrons lose on average only 1% of their energy with each elastic scatter; therefore, the neutron energy loss is nearly continuous.[7] Between energies of ~ 0.1 eV and 10 keV, a very simple equation can be used to describe the relationship between neutron energies and elapsed time in the neutron spectrometer[10]:

$$E_{avg} = \frac{k}{(t+t_0)^2}\ ,\ 0.1\ \text{eV} < E_{avg} < 10\ \text{keV}\ , \qquad (1)$$

where

E_{avg} = mean energy of the interrogation neutrons

t = elapsed time after the neutron pulse is injected

t_o, k = system-dependent constants having units of eV·μs^2 and μs, respectively.

Below 0.1 eV, the resolution of the neutron energy distribution broadens, and Eq. (1) is no longer valid due to effects from the thermal vibrations of the lead medium.[10]

As the interrogating neutrons slow down in the lead, they induce fissions in the various isotopes of the sample, located in the LSDS channel shown in Fig. 1. These fissions release prompt neutrons that contribute to the time-dependent signal generated in the assay detectors (e.g., fission chambers containing either ^{232}Th or ^{238}U). One can distinguish the fission neutrons from the interrogation neutrons by their higher energy in the slowing-down-time region of interest (i.e., $t > 10$ μs). As ^{232}Th and ^{238}U have very low fission cross sections (<100 μb) below 100 keV, they make ideal materials for assay chambers to detect the more energetic neutrons emitted from the fissions.

The different algorithms require different detectors. Both the linear and quadratic empirical models discussed in this paper rely entirely on the signal from these assay detectors. In contrast, the semiempirical algorithm relies on the isotopic fission chambers in addition to the assay detectors. Isotopic fission chambers are mostly sensitive to the interrogation neutron flux and are lined with fissile isotopes (e.g., ^{235}U, ^{239}Pu, and ^{241}Pu) that are also assumed to be present in the sample. One can use these isotopic fission chambers to provide energy-broadened, time-dependent fission cross sections to deconvolve the assay signal from the assay detectors.

For samples sufficiently small that the neutron self-shielding is negligible, the signals from the assay detectors can be expressed as a linear combination of the signals from these isotopic fission chambers, as given by

$$y(t) = C\sum_i a_i x_i(t)\ ,\ i = {}^{235}\text{U}\ ,\ {}^{239}\text{Pu}\ ,\ {}^{241}\text{Pu}\ , \qquad (2)$$

where

$y(t)$ = response from the assay detector

C = constant that is used to account for the different efficiencies of the threshold assay chambers and the isotopic fission chambers

$x_i(t)$ = responses from the isotopic fission chambers.

The isotopic constants a_i are related to their respective masses in the sample m_i by

$$a_i \propto \frac{m_i \bar{\nu}_i N_i}{A_i}\ , \qquad (3)$$

where

A_i = atomic weight of the fissile isotope

$\bar{\nu}_i$ = average number of neutrons emitted per fission of isotope i

N_i = number of fissile atoms used in the isotopic fission chamber.[11]

III. EXPERIMENT SETUP

The Gaerttner LINAC Center at RPI has been performing nuclear data experiments since 1961 to improve neutron data libraries.[12] These measurements, which require a high-yield, pulsed neutron source, are driven by the LINAC. For assay experiments with the LSDS, the electron linear accelerator at Gaerttner is tuned to a pulse frequency of 180 Hz, an electron current of 15 μA, and an electron energy of 50 MeV. The electrons from the LINAC interact with a gas-cooled tantalum target located in the center of the lead cube to produce neutrons via bremsstrahlung radiation (e,γ). Approximately 0.03 neutrons are produced per incident electron, which results in a neutron intensity of 1.6×10^{10} n/pulse. Therefore, a typical 60-min experiment produces $\sim 1 \times 10^{16}$ neutrons. The energy spectrum of these neutrons can be represented by an evaporation spectrum with an average neutron energy of 0.46 MeV (Ref. 13):

$$\phi(E) = E \cdot \exp\left(-\frac{E}{0.46}\right), \quad (4)$$

where E is the energy of the neutrons.

III.A. The RPI LSDS

The slowing-down spectrometer at RPI is a 1.8-m cube of high-purity lead weighing ~66 tonnes, displayed in Fig. 1. The faces of the LSDS are covered with 0.75-mm-thick sheets of cadmium, which prevent thermal neutrons from reentering the LSDS. An interrogation channel (15- × 15-cm opening) through the lead contains an aluminum assembly used to hold the fissile samples and assay detectors. Additionally, assay detectors are mounted in the lead above the assembly. There are small ports in the upper corners of the lead for external flux monitors used to normalize independent experiments to standard beam conditions.

III.B. Neutron Detection Systems

Two types of fission chambers, one lined with ^{232}Th and the other lined with ^{238}U, were both used as assay detectors to observe the induced fission signal. These detectors were manufactured by Westinghouse with an active length of 20 cm and a diameter of 2.5 cm. Each is composed of ~200 mg of fissionable material. The ^{238}U detector contains highly depleted uranium, with a residual ^{235}U composition of 4.1 ppm. The ^{232}Th detector contains even less fissile material (<25 ppb ^{235}U), which improves the signal-to-noise ratio; however, because of the relatively small ^{232}Th fission cross section, the ^{238}U detector is about three times as efficient.[14] These detectors were placed near the fissile samples to detect fission neutrons induced by the interrogation flux. A second ^{238}U fission chamber, also containing 200 mg of highly depleted uranium, was positioned in the lead.

The neutron flux produced by the LINAC was monitored with a ^{235}U fission chamber, positioned in the upper corner of the RPI LSDS. This flux monitor contains ~1.0 mg of fissile material and is intended to serve as a means to normalize the assay detector responses to standard LINAC conditions. The two isotopic fission chambers (^{235}U and ^{239}Pu) for implementation of the semiempirical algorithm were positioned in the interrogation channel. They contained 1.0 and 0.3 mg for the ^{235}U and ^{239}Pu fission chambers, respectively. Overall, six fission chambers were utilized for LSDS assay experiments.

A diagram of the instrumentation for a fission chamber is shown in Fig. 2. The preamplifier provides the direct-current, high-voltage power required by the

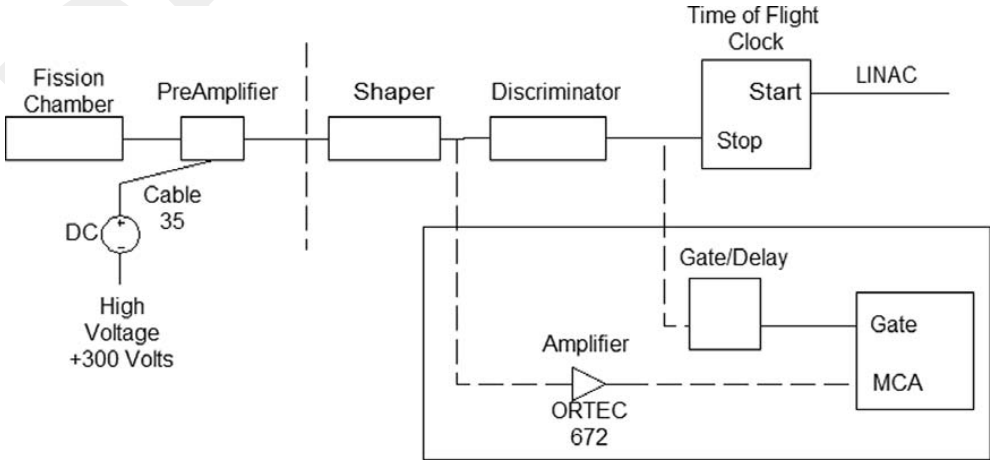

Fig. 2. Diagram of nuclear instrumentation used to collect data and in the boxed region to calibrate the discrimination for assay detectors.

fission chamber as well as decouples the transient detector signal. The decoupled detector signal is amplified and passed to a 100-ns Gaussian shaping amplifier. A calibrated constant fraction discriminator was used to differentiate fissions from background events. The primary source of background is alpha radiation emitted within the fission chambers, which deposits significantly less energy than fission events. A diagram representing the electronic configuration used to calibrate the system is shown by the boxed portion of Fig. 2.

The time spectra were recorded with a time-of-flight clock (FAST ComTec MCS6). The clock was triggered by a pretrigger signal from the LINAC, indicating the start of each neutron pulse (t_0). The clock was stopped by the fission response of the detectors, and the resulting time information was discretized into 409.6-ns-wide time bins. The spectra were corrected for the detector dead time by applying a dead-time correction. Additionally, the measured slowing-down-time spectra were corrected for the delay between the LINAC trigger (t_0) and the time of the actual neutron pulse. Finally, the collected spectra were grouped into larger, logarithmically spaced time bins.

The experiments involved the assay of both fissile plutonium and uranium. Measurements were performed with a variety of fissile samples, including a fresh SPERT fuel pin, 10 highly enriched uranium (HEU) disks, and two plutonium-beryllium (PuBe) neutron sources. Table I describes these samples. Combinations of these samples were used to measure the response to variable quantities of ^{239}Pu in the presence of different masses of ^{235}U.

These measurements involved numerous experimental setups, which were altered between LINAC runs. At the start of each day, a background measurement was performed. Subsequent experiments with fissile samples involved 30 min of data collection, with enough cool-down time between experiments to allow for safe sample changing. Examples of the time spectra collected are shown in Fig. 3, which shows the count rate from the ^{238}U assay detector for various quantities of plutonium and the SPERT fuel pin. In the analysis, time spectra from 28 to 2600 μs were used. This range corresponds to ~200 and 0.02 eV, respectively.

TABLE I

Fissile Specimens Assayed in Recent RPI LSDS Experiments

Sample	Isotope	Mass (g)
SPERT fuel pin	^{235}U	34.7 ± 0.2
Large ^{239}PuBe source	^{239}Pu	91 ± 5
Small ^{239}PuBe source	^{239}Pu	47 ± 2
Five HEU disks (one through five)	^{235}U	1.2039 ± 0.0006
Ten HEU disks (one through ten)	^{235}U	2.455 ± 0.001

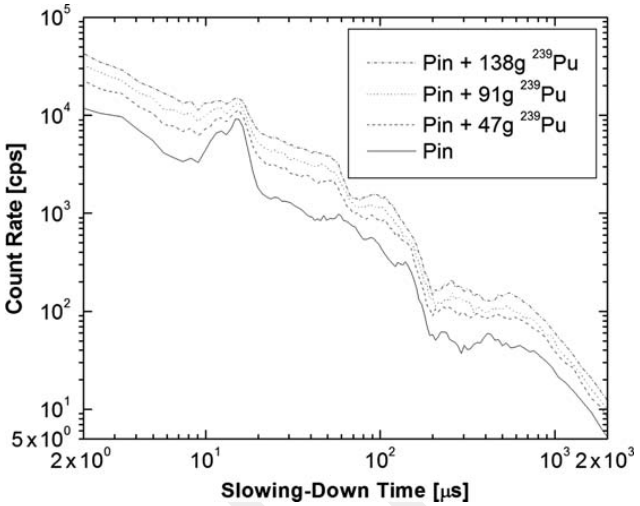

Fig. 3. Normalized count rate versus slowing-down time recorded by the ^{238}U threshold fission chamber in the lead for a fresh SPERT fuel pin with various amounts of plutonium. The curves are normalized to standard LINAC beam conditions.

The uncertainty of assay measurements with the LSDS system is split into two categories: statistical uncertainty and systematic error. The former is improved by taking longer experimental measurements. Assuming average beam conditions, the aggregate neutron production will achieve 10^{16} neutrons in 1 h of continuous operation. Therefore, the LINAC-driven LSDS assay system can match the source strength required for adequate statistical certainty for the PNNL algorithms in a measurement ~30 min long.

Systematic uncertainty is more difficult to quantify and is primarily due to variable beam conditions, detector dead-time corrections, and positioning of the detectors and samples. The issue of variable beam conditions is treated by normalizing individual experiments with external flux monitors. The detector dead time is accounted for by applying a dead-time correction, which assumes an exponential behavior between pulses. This dead-time correction factor remained <5% for the entire spectrum and dropped to <2% after 50 μs. This correction method has a relative uncertainty of <1% for a dead time of <5% (Ref. 15). Last, the uncertainty in detector and sample positioning for these measurements is of concern because small alterations in position can impact the fission chamber signal, which in turn affects the calculated fissile mass. Therefore, it is necessary to accurately measure and secure the position of such samples and detectors when performing experiments. Overall, the systematic uncertainty of the RPI LSDS is conservatively estimated to be <2% (Ref. 15).

IV. ANALYSIS ALGORITHMS

The effect of self-shielding due to the presence of large quantities of neutron-absorbing isotopes in our samples invalidates the use of Eq. (2) to determine the fissile isotopic masses in the samples.[16] The nonlinearity caused by this self-shielding and the complexity of the fuel assembly geometry, such as neutron streaming paths between the fuel rods, has guided us to develop algorithms that are more empirical in nature to achieve sufficient accuracy in the estimated masses.

All three of the algorithms described in this work are based on maximum likelihood estimation (MLE) to estimate the isotopic masses.[8] The MLE approach assumes a Poisson counting statistics model for the measured assay signals. It involves minimizing an objective function R (the negative log-likelihood function) given by

$$R = \sum_{j=1}^{n} \left\{ y'(t_j) - y(t_j) \ln\left[y'(t_j) \right] \right\} , \tag{5}$$

where

t_j = the j'th bin of the slowing-down time

y' = calculated assay signal

y = measured assay signal as previously defined.

IV.A. Semiempirical Algorithm

For the semiempirical algorithm, we accounted for the effects of self-shielding by multiplying the right side of Eq. (2) by a self-shielding function $f(t)$ to obtain

$$y(t) = f(t) C \sum_i a_i x_i(t) , \tag{6}$$

where we define $f(t)$ as

$$f(t) = \frac{\bar{\phi}_{fuel}(E,t)}{\bar{\phi}_{detectors}(E,t)} , \tag{7}$$

where $\bar{\phi}_{fuel}(E,t)$ and $\bar{\phi}_{detectors}(E,t)$ are the average neutron fluxes over the fuel assembly and the detectors, respectively. Note that in the notation of $f(t)$, we have suppressed the dependency on the isotopic masses m_i of the fuel assembly. The assay response $y(t)$ can be measured with threshold fission chambers lined with ^{232}Th or ^{238}U, while the isotopic responses $x_i(t)$ can be measured with fissile isotopic fission chambers separately lined with ^{235}U, ^{239}Pu, and ^{241}Pu. In Eq. (7), we assumed that $\bar{\phi}_{fuel}(E,t)$ and $\bar{\phi}_{detector}(E,t)$ have the same energy dependence so that $f(t)$ is independent of energy. This assumption is not strictly valid, since one would expect that $\bar{\phi}_{fuel}(E,t)$ would be skewed toward higher energies than $\bar{\phi}_{detector}(E,t)$ due to the higher absorption rate for lower-energy neutrons in the fuel. Based on previous work discussed in Ref. 4, we believe this assumption to be valid to better than 1%.

The semiempirical algorithm relies on a calibration set of fissile samples for which the masses are assumed to be known with small uncertainty, $\sim$1%. This calibration set must be carefully chosen to incorporate as much variability as possible while minimizing the size of the set. Each LSDS assay of a sample in the calibration set yields $y(t)$ and corresponding $x_i(t)$'s. The masses in the calibration set are well-known and can be used to determine the corresponding a_i for each isotope in the corresponding sample by solving Eq. (3) for a_i. We then substitute the $y(t)$, $x_i(t)$'s, and $a_i(t)$'s into Eq. (6) and solve for $f(t)$. The $f(t)$'s from the calibration set were used to form a matrix, and SVD (Ref. 17) was applied to this matrix to obtain a set of orthogonal basis vectors. We then approximate the $f(t)$'s of samples for which the isotopic masses are unknown using linear combinations of these basis vectors. Previous literature provides a more detailed mathematical description of this approach.[5] We describe this approach as semiempirical because it retains the physics model described by the summation term in Eq. (6) while relying on an empirical fit to account for self-shielding effects as well as other assumptions that cannot easily be modeled (e.g., light-element impurities in the lead). We retained the physics model in order to reduce the amount of variability required of the calibration set and empirical fitting procedure. Application of the semiempirical algorithm to detailed Monte Carlo simulations of LSDS assays has demonstrated the potential of LSDS to estimate the sum of ^{239}Pu and ^{241}Pu mass in used-fuel assemblies with $<2\%$ relative error, on average.[5]

IV.B. Linear Empirical Algorithm

The semiempirical algorithm requires isotopic fission chambers that are separately lined with ^{235}U, ^{239}Pu, and ^{241}Pu. Obtaining such plutonium-based fission chambers, particularly lined with ^{241}Pu, is difficult. Therefore, we developed algorithms that do not rely on the use of these isotopic fission chambers. The linear and quadratic algorithms are purely empirical and do not rely on a physical model. Consequently, one can use them to estimate the masses of nonfissile, neutron-absorbing isotopes in the fuel that also impact the assay signal, such as ^{240}Pu. The IAEA includes ^{240}Pu in its definition of total plutonium.

The concept of the empirical algorithms is to use linear algebra to relate a vector of the isotopic masses in the used fuel to a vector corresponding to the counts in the time bins of the assay signal. For the linear empirical model, the vector m consisting of p isotopic masses is related to the vector y consisting of the n slowing-down time bins via

$$y = Bm + e , \tag{8}$$

where B is an $n \times p$ matrix of parameters to be determined and e is a vector of n offsets. The offsets

are residuals from the fit of the model-estimated assay signal to the measured assay signal.

The matrix B is determined by fitting a set of measured assay signals from the calibration fuel assemblies. The relationship between the known assay signals and the known assay masses is similar to Eq. (8) except that the assay signals, masses, and offsets are now matrices:

$$Y = BM + E \,, \tag{9}$$

where

Y = $n \times k$ matrix formed from the assay signals obtained by performing LSDS measurements on the k calibration assemblies

$Y = [y_1(t)\ y_2(t)\ \ldots\ y_k(t)]$

M = $p \times k$ matrix of the known p isotopic masses of interest in the k calibration assemblies

E = $n \times k$ matrix of the n offsets (error residuals from the fitting) for the k calibration assemblies.

Eq. (9) is then solved for matrix B using MLE.

IV.C. Quadratic Empirical Algorithm

The quadratic empirical algorithm is a simple extension of the linear empirical algorithm. It was developed to more accurately account for the nonlinear effects caused by self-shielding. For this algorithm, the vector y of n time bins of the assay signal is related to the vector m of p masses and the vector q of p masses squared by

$$y = Cm + Dq + e \,, \tag{10}$$

where C and D are $n \times p$ matrices of parameters. The matrices C and D are determined through the calibration procedure. Extending the notation used in Eq. (9), we use MLE to obtain the matrices C and D by solving

$$Y = CM + DQ + E \,, \tag{11}$$

where Q is a $p \times k$ matrix containing the squares of the known masses of the calibration set. The cross-terms are currently neglected, since including them would require a larger calibration set.

IV.D. Considerations for Application of Algorithms to Experimental Data

Certain factors must be addressed when applying the algorithms to experimental data. For instance, it is not possible to control the LINAC perfectly in such a way that it serves as a consistent neutron source from experiment to experiment. Therefore, it is necessary to normalize each detector to minimize fluctuations in detector signals resulting from variations in neutron fluence. This is particularly important for the first- and second-order empirical algorithms, which rely entirely on the assay detector signal. Ideally, the detector signals at RPI are normalized by the signal of the ^{235}U flux monitor situated in the lead away from the LSDS channel, as shown in Fig. 1. Unfortunately, during the 2012 measurements, the signal from the ^{235}U flux monitor had unusually high noise levels for some of the assays. Therefore, for these measurements, the ^{239}Pu fission chamber signal was used to normalize the signals from the other detectors.

Other considerations had to be accounted for when applying algorithms that rely on calibration. The fission chambers are quite small, so variation in sample position with respect to the detectors manifests itself in additional variation in the amplitude of the detector signals from measurement to measurement. Spurious results were obtained when applying the algorithms to data for which it was known that the assay samples were not situated consistently. Therefore, the analysis that was performed on this particular data set is not reported. Although background measurements were taken for which there was no assay sample in the LSDS channel, we observed that the background signal was negligible.

V. RESULTS

In August and September of 2012, RPI ran a set of measurements using samples consisting of combinations of the following items[18]:

1. a fresh UO_2 SPERT fuel pin, having a ^{235}U enrichment of 4.8 wt% (34.8 g of ^{235}U)
2. ten highly enriched (93.3%) ^{235}U (HEU) disks, with each disk having a diameter of $\sim$1.27 cm and containing between 0.2 and 0.3 g of ^{235}U; the disks were combined into two packages of five disks each, both with 1.3 g of ^{235}U
3. a small PuBe source containing $\sim$47 g of ^{239}Pu
4. a large PuBe source containing $\sim$91 g of ^{239}Pu.

PNNL analyzed the data from these experiments using the first- and second-order empirical models as well as the semiempirical model. The set of calibration measurements shown in Table II was used for all three algorithms. As mentioned in Sec. IV, the measurements were normalized using the ^{239}Pu fission chamber because the ^{235}U flux monitor was performing erratically. For the quadratic empirical fit, only the ^{239}Pu mass was allowed to vary quadratically. Results for the ^{235}U mass estimates of the test-case samples used in these experiments are presented in Table III. The true masses as well as the relative difference of the extracted masses from the algorithms and the true masses are reported. Results for the ^{239}Pu mass estimates of the test-case samples used in

TABLE II

Calibration Set Used for Analysis of Experimental Data

Assay Target	^{235}U Mass (g)	^{239}Pu Mass (g)
Pin	34.8	0
Pin + ten disks	37.4	0
Pin + small PuBe	34.8	47
Pin + five disks + large PuBe	36.1	91
Pin + ten disks + both PuBe	37.4	138

this second batch of experiments are presented in Table IV.

Of the three algorithms, the linear empirical algorithm performed the best, estimating the ^{235}U mass over the seven test cases to a root-mean-square error (RMSE) of 2.7% and the ^{239}Pu mass to 6.3% RMSE. The other algorithms performed significantly worse, with up to twice the RMSE for the ^{235}U estimates. The poorer estimates of the ^{239}Pu masses compared to the ^{235}U masses could be due to the much larger range in actual ^{239}Pu masses used in the measurements and/or the use of the ^{239}Pu fission chamber rather than the ^{235}U flux monitor to normalize the neutron fluence. The ^{239}Pu fission chamber was placed in the assay channel during the measurements, while the ^{235}U flux monitor was situated in the lead farther away from the fissile samples, as shown in Fig. 1. Therefore, the ^{239}Pu fission chamber would be exposed to more fast neutrons from fissions within the sample than the ^{235}U flux monitor.

The quadratic empirical algorithm performed significantly worse than the linear empirical algorithm. For the quadratic algorithm, only the ^{239}Pu mass was allowed to vary quadratically. The poorer performance of the quadratic algorithm suggests that nonlinear affects are not statistically significant for the geometries of these measurements.

Of the three algorithms, the semiempirical algorithm performed the worst. Its relatively poor performance on these experiments is a significant departure from its performance for simulations of fuel assemblies. It is

TABLE III

Results for ^{235}U Mass Estimates on Test-Case Samples for Second Batch of Experimental Data

Assay Target	True ^{235}U Mass (g)	Relative Error (%)		
		Linear	Quadratic	Semiempirical
Pin + five disks	36.1	1.6	2.5	11.3
Pin + five disks + small PuBe	36.1	−3.1	−0.3	16.9
Pin + ten disks + small PuBe	37.4	0.3	3.0	11.2
Pin + large PuBe	34.8	0.4	6.0	−0.3
Pin + ten disks + large PuBe	37.4	−0.6	4.9	0.3
Pin + both PuBe	34.8	1.8	−2.6	−11.9
Pin + five disks + both PuBe	36.1	−6.0	−10.0	−9.7
RMSE	—	2.7	5.1	10.4

TABLE IV

Results for ^{239}Pu Mass Estimates on Test-Case Samples for Second Batch of Experimental Data

Assay Target	True ^{239}Pu Mass (g)	Relative Error (%)		
		Linear	Quadratic	Semiempirical
Pin + five disks	0	—	—	—
Pin + five disks + small PuBe	47	−7.9	−13.2	−11.9
Pin + ten disks + small PuBe	47	−10.1	−16.2	−11.7
Pin + large PuBe	91	8.2	1.8	16.5
Pin + ten disks + large PuBe	91	1.6	−5.3	4.0
Pin + both PuBe	91	1.9	5.5	2.4
Pin + five disks + both PuBe	138	1.2	4.4	3.2
RMSE	—	6.3	9.3	9.9

unclear why the semiempirical algorithm performed so poorly. We conjecture that the fundamental assumption of the semiempirical model, namely, that the ratio of the average flux at the sample to the flux at the detectors is related to the isotopic masses of the sample, is not appropriate for the measurement geometries examined to the high level of accuracy required.

The impact of background in the fission chamber signals was investigated. Background measurements were conducted at least once per day. These measurements involved recording the signals from the fission detectors while the LINAC was producing neutrons in the lead spectrometer with no sample in the assay chamber. The mass estimates in Tables III and IV were determined without background subtraction. The analysis was repeated with background subtraction, but the results did not improve.

The composition of the measurement samples presents challenges for translating these results into expectations of performance for the algorithms when applied against used-fuel assemblies. First, the range of ^{235}U masses among the samples is relatively small, 34.8 to 37.4 g. If one randomly guessed the ^{235}U mass assuming a flat distribution between the lowest and highest mass of the sample set, one would have achieved an RMSE of 3.4%, which is only slightly larger than the RMSE of the linear model. Note that the direct comparison of uncertainties of a bounded random guess to the applied algorithms is misleading, since no bounds on the masses were applied for the algorithms. Second, the integrated counts of the time spectra are sensitive to the total fissile mass of the sample, and there is significant variation in the total fissile mass among the samples measured. It is likely that the empirical algorithms were able to take advantage of this dependence in estimating the masses. It is unclear how this dependence will translate to performance on used-fuel assemblies that have similar total fissile masses.

VI. CONCLUSIONS

The linear and quadratic empirical algorithms, along with a semiempirical algorithm, were applied to experimental data taken with the LSDS located at RPI Gaerttner Linear Accelerator Center. These algorithms previously had been successfully tested against simulation-based results.[8] This paper reports the first attempt to apply our algorithms to data. The linear empirical algorithm achieved RMSEs of 2.7% and 6.3% for the ^{235}U mass and ^{239}Pu mass of seven different geometries using five other geometries as a calibration set. Significant effort is yet needed to demonstrate the applicability of these algorithms for used-fuel assemblies; these measurements do not allow for the evaluation of the effect of self-shielding due to large quantities of materials. Despite this shortcoming, the results reported here are encouraging in demonstrating that we are making progress toward the goal of assay of used-fuel assemblies.

Recently, the collaboration has focused efforts on planning for a larger experimental demonstration of LSDS. Because of the radiation safety hazards associated with handling used-fuel assemblies, it will not be possible to demonstrate LSDS for used-fuel-assembly assay in the near term (within $\sim$2 years). Instead, the near-term demonstration will likely include the assay of a fresh-fuel subassembly and an array of mixed oxide (MOX) fuel pins. The fresh subassembly assay will provide knowledge regarding the ability of the detectors and electronics to operate effectively (e.g., manage dead-time and pile-up issues) with high count rates as well as to study self-shielding further in more realistic geometries. An assay of MOX fuel pins will provide an opportunity to quantify ^{235}U and ^{239}Pu mass when present in the same sample. Also, the MOX fuel pins are all of the same geometry and have similar total mass, which should provide a more relevant test of the algorithms for the intended LSDS application in which the geometry of the samples is not variable for a given calibration set.

REFERENCES

1. N. PETER, "A Shipper-Receiver-Difference Approach for Reprocessing Plants," *Proc. 8th Int. Conf. Facility Operations–Safeguards Interface*, Portland, Oregon, March 30–April 4, 2008.

2. L. E. SMITH et al., "AFCI Safeguards Enhancement Study: Technology Development Roadmap," PNNL-18099, Pacific Northwest National Laboratory (2008).

3. Y. DANON et al., "Measurements with the High Flux Lead Slowing-Down Spectrometer at LANL," *Nucl. Instrum. Methods Phys. Res., Sect. B*, **261**, 953 (2007); http://dx.doi.org/10.1016/j.nimb.2007.04.013.

4. C. ROMANO et al., "Measurements of (n,α) Cross-Section of Small Samples Using a Lead-Slowing-Down-Spectrometer," *Nucl. Instrum. Methods Phys. Res., Sect. A*, **562**, 771 (2006); http://dx.doi.org/10.1016/j.nima.2006.02.052.

5. J. KULISEK et al., "Assaying Used Nuclear Fuel Assemblies Using Lead Slowing-Down Spectroscopy and Singular Value Decomposition," *IEEE Trans. Nucl. Sci.*, **60**, 539 (2013); http://dx.doi.org/10.1109/TNS.2013.2250304.

6. D. B. PELOWITZ, "MCNPX User's Manual, Version 2.60," LA-CP-07-1473, Los Alamos National Laboratory (2008).

7. M. L. FENSIN et al., "A Monte Carlo Based Spent Fuel Analysis Safeguards Strategy Assessment," LA-UR 09-01632, Los Alamos National Laboratory (2009).

8. J. KULISEK et al., "Lead Slowing-Down Spectrometry Time Spectral Analysis for Spent Fuel Assay: FY12 Status Report," PNNL-21970, Pacific Northwest National Laboratory (Oct. 2012).

9. B. BECKER et al., "Nondestructive Assay Measurements Using the RPI Lead Slowing-Down Spectrometer," *Nucl. Sci. Eng.*, **175**, 124 (2013); http://dx.doi.org/10.13182/NSE12-66.

10. Y. D. LEE et al., "Design of a Spent-Fuel Assay Device Using a Lead Spectrometer," *Nucl. Sci. Eng.*, **131**, 45 (1999); http://dx.doi.org/10.13182/NSE97-100.

11. L. E. SMITH et al., "Time-Spectral Analysis Methods for Spent Fuel Assay Using Lead Slowing-Down Spectroscopy of Spent Fuel," *IEEE Trans. Nucl. Sci.*, **57**, 2230 (2010); http://dx.doi.org/10.1109/TNS.2010.2051958.

12. E. R. GAERTTNER, M. L. YEATER, and R. R. FULLWOOD, "Rensselaer Polytechnic Institute Linac Facility," *Proc. Symp. Neutron Physics*, Troy, New York, May 5–6, 1961.

13. N. M. ABDURRAHMAN et al., "Spent-Fuel Assay Performance and Monte Carlo Analysis of the Rensselaer Slowing-Down-Time Spectrometer, *Nucl. Sci. Eng.*, **115**, 279 (1993); http://dx.doi.org/10.13182/NSE92-94.

14. D. S. CRAMER et al., "Lead Spectrometer for Non-Destructive Nuclear Fuel Assay," KAPL-M-7449, Knolls Atomic Power Laboratory (July 1976).

15. N. M. ABDURRAHMAN, "System Performance and Monte Carlo Analysis of Light Water Reactor Spent Fuel Assay Using Neutron Slowing Down Time Method," Doctoral Thesis, Rensselaer Polytechnic Institute (1991).

16. L. E. SMITH et al., "Lead Slowing-Down Spectroscopy for Direct Measurement of Plutonium in Spent Fuel: NGSI Phase I Report," PNNL-20158, Pacific Northwest National Laboratory (2011).

17. G. H. GOLUB and C. REINSCH, "Singular Values and Least Squares Solutions," *Numer. Math.*, **14**, 403 (1970); http://dx.doi.org/10.1007/BF02163027.

18. A. WELTZ et al., "Non-Destructive Assay of Plutonium and Uranium with the RPI LSDS," *Trans. Am. Nucl. Soc.*, **108**, 142 (2013).